Supporting Information

Charge-Transfer Interactions Govern the Trans Influence and Electron-Induced Bond Activation in Linear Au(I) Complexes

Akef T. Afaneh[1*], Mansour H. Almatarneh[2,4], Ibrahim A. Daboubash[1], Ali Marashdeh[1,3] and Oqab M. Abu Rumman[2]

[1]Department of Chemistry, Faculty of Science, Al-Balqa Applied University, 19117 Al-Salt, Jordan. [2]Department of Chemistry, The University of Jordan, Amman 11942, Jordan. [3]Leiden Institute of Chemistry, Gorlaeus Laboratories, Leiden University, Leiden, The Netherlands. [4]Department of Chemistry, College of Science, Imam Mohammad Ibn Saud Islamic University (IMSIU), Riyadh 11623, Saudi Arabia.

Neutral $XAuChMe_2$ (Ch = O, S, Se and Te)

$ClAuOMe_2$

79	0.254920000	-0.000016000	-0.044057000
17	2.491843000	0.000036000	0.128138000
8	-1.886416000	0.000016000	-0.238281000
6	-2.578459000	-1.198715000	0.149545000
1	-3.587218000	-1.174787000	-0.265630000
1	-2.024694000	-2.034893000	-0.264329000
1	-2.621850000	-1.280168000	1.236962000
6	-2.578420000	1.198773000	0.149528000
1	-2.024629000	2.034928000	-0.264360000
1	-3.587181000	1.174872000	-0.265643000
1	-2.621806000	1.280245000	1.236945000

$BrAuOMe_2$

79	-0.093016000	0.000005000	-0.061375000
35	2.268273000	0.000000000	0.081744000
6	-2.943760000	-1.198063000	0.178176000
1	-3.957022000	-1.178184000	-0.226509000
1	-2.392954000	-2.034782000	-0.238853000
1	-2.976617000	-1.277511000	1.266271000
6	-2.943862000	1.198012000	0.178186000
1	-2.393206000	2.034781000	-0.238946000
1	-3.957166000	1.177987000	-0.226384000
1	-2.976606000	1.277521000	1.266280000
8	-2.257750000	0.000011000	-0.219056000

$IAuOMe_2$

79	-0.401124000	0.000002000	-0.070687000
53	2.124097000	-0.000001000	0.059742000
6	-3.283131000	-1.196845000	0.195591000
1	-4.297307000	-1.182930000	-0.207702000
1	-2.730914000	-2.034398000	-0.218371000
1	-3.315747000	-1.273582000	1.284149000

6	-3.283158000	1.196829000	0.195596000
1	-2.730968000	2.034396000	-0.218373000
1	-4.297338000	1.182887000	-0.207688000
1	-3.315768000	1.273566000	1.284154000
8	-2.600320000	0.000001000	-0.205667000

$ClAuSMe_2$

79	0.403106000	0.000029000	-0.079089000
16	-1.866789000	-0.000013000	-0.476296000
6	-2.569328000	-1.398922000	0.462069000
1	-2.275950000	-1.347337000	1.506467000
1	-3.652326000	-1.374110000	0.360802000
1	-2.178478000	-2.307946000	0.013671000
6	-2.569395000	1.398820000	0.462132000
1	-2.178572000	2.307882000	0.013789000
1	-3.652389000	1.373966000	0.360849000
1	-2.276029000	1.347181000	1.506531000
17	2.651136000	-0.000065000	0.268322000

$BrAuSMe_2$

79	0.051004000	0.000103000	-0.119002000
16	-2.245682000	-0.000052000	-0.442371000
6	-2.912131000	-1.399467000	0.520863000
1	-2.580301000	-1.348093000	1.553730000
1	-3.998196000	-1.376066000	0.460085000
1	-2.537317000	-2.308084000	0.058112000
6	-2.912352000	1.399099000	0.521096000
1	-2.537656000	2.307850000	0.058513000
1	-3.998411000	1.375550000	0.460288000
1	-2.580537000	1.347584000	1.553960000
35	2.430883000	-0.000111000	0.173791000

$IAuSMe_2$

79	-0.263490000	0.000168000	-0.141971000
53	2.285686000	-0.000115000	0.128344000
16	-2.590558000	-0.000083000	-0.419742000
6	-3.230210000	-1.399994000	0.560315000
1	-4.317549000	-1.378199000	0.529636000
1	-2.867339000	-2.308214000	0.087340000
1	-2.870428000	-1.349154000	1.583839000
6	-3.230585000	1.399370000	0.560721000
1	-2.867940000	2.307824000	0.088021000
1	-4.317916000	1.377301000	0.530014000
1	-2.870809000	1.348317000	1.584237000

$ClAuSeMe_2$

79	0.661455000	0.000051000	-0.054812000
34	-1.723867000	-0.000014000	-0.407750000
17	2.922225000	-0.000111000	0.245483000

6	-2.370056000	-1.480515000	0.717966000
1	-1.969623000	-1.380284000	1.720959000
1	-3.456299000	-1.456216000	0.719856000
1	-2.013748000	-2.398654000	0.261015000
6	-2.370188000	1.480338000	0.718086000
1	-3.456427000	1.455921000	0.719995000
1	-1.969726000	1.380077000	1.721065000
1	-2.013989000	2.398550000	0.261196000

$BrAuSeMe_2$

79	-0.320353000	0.000007000	-0.094541000
34	2.087922000	0.000000000	-0.382689000
6	2.697749000	1.480789000	0.762517000
1	2.265255000	1.381110000	1.752176000
1	3.783358000	1.456868000	0.799541000
1	2.356226000	2.398731000	0.293998000
6	2.697699000	-1.480826000	0.762492000
1	3.783310000	-1.456926000	0.799532000
1	2.265194000	-1.381171000	1.752149000
1	2.356174000	-2.398751000	0.293940000
35	-2.710392000	-0.000005000	0.161108000

$IAuSeMe_2$

79	-0.011820000	0.000192000	-0.118099000
6	3.006185000	-1.481439000	0.792510000
1	2.676284000	-2.398980000	0.314905000
1	4.090540000	-1.457861000	0.856229000
1	2.549749000	-1.383225000	1.771549000
6	3.006562000	1.480791000	0.792989000
1	2.550085000	1.382383000	1.771989000
1	4.090908000	1.456900000	0.856714000
1	2.676911000	2.398574000	0.315674000
53	-2.569306000	-0.000133000	0.119910000
34	2.423411000	-0.000060000	-0.365456000

$ClAuTeMe_2$

79	0.904739000	0.000018000	-0.041331000
52	-1.630036000	-0.000001000	-0.371151000
6	-2.234695000	1.593648000	0.961107000
1	-1.901658000	2.525758000	0.514769000
1	-3.317225000	1.577439000	1.044822000
1	-1.758788000	1.446202000	1.924307000
6	-2.234625000	-1.593728000	0.961046000
1	-1.758750000	-1.446275000	1.924260000
1	-3.317159000	-1.577601000	1.044740000
1	-1.901514000	-2.525799000	0.514686000
17	3.179911000	-0.000036000	0.239086000

$BrAuTeMe_2$

79	-0.572821000	0.000003000	-0.082359000
52	1.981281000	0.000002000	-0.350600000
6	2.548262000	-1.594121000	0.997637000
1	2.228996000	-2.526100000	0.541090000
1	3.627874000	-1.577271000	1.112754000
1	2.044483000	-1.447843000	1.946729000
6	2.548286000	1.594095000	0.997657000
1	2.044486000	1.447829000	1.946740000
1	3.627896000	1.577205000	1.112791000
1	2.229059000	2.526089000	0.541113000
35	-2.975881000	-0.000002000	0.158989000

$IAuTeMe_2$

79	-0.269335000	0.000011000	-0.107681000
52	2.308454000	-0.000005000	-0.336078000
6	2.845969000	-1.594668000	1.023657000
1	2.538872000	-2.526511000	0.558546000
1	3.922465000	-1.576734000	1.164553000
1	2.319490000	-1.450356000	1.960661000
6	2.845952000	1.594657000	1.023669000
1	2.319485000	1.450324000	1.960675000
1	3.922451000	1.576748000	1.164556000
1	2.538832000	2.526496000	0.558566000
53	-2.839156000	-0.000009000	0.119459000

SI.1 Structural Analysis. Linear Au(I) reference halides exhibit Au–X distances on the order of ~2.2 Å (Cl), ~2.34 Å (Br), and ~2.5 Å (I) in the gas phase.[1-5] In the present X–Au–L series, the optimized geometries remain essentially linear at Au (X–Au–L ≈ 179° for all complexes; Fig. SI.1)[4, 6-11], and Au–X follows the expected halide trend Cl < Br < I for each fixed donor L. Consistent with trans influence, Au–X also lengthens slightly as the donor is varied from OMe_2 → SMe_2 → $SeMe_2$ → $TeMe_2$: for example, Au–X increases from 2.244/2.366/2.529 Å (L = OMe_2) to 2.292/2.415/2.580 Å (L = $TeMe_2$) for X = Cl/Br/I, respectively. In parallel, Au–L increases monotonically with chalcogen size and donor softness/polarizability, with Au–L spanning 2.150–2.203 Å (OMe_2), 2.304–2.344 Å (SMe_2), 2.411–2.448 Å ($SeMe_2$), and 2.556–2.588 Å ($TeMe_2$) across X = Cl/Br/I. The internal ligand angle also evolves systematically: the C–Ch–C angle decreases from ~113° (O) to ~100° (S) to ~98° (Se) and ~95–96° (Te), consistent with increasingly diffuse lone pairs and reduced hybridization as the chalcogen becomes heavier. Across a fixed donor L, the expected trend Au–L(Cl) < Au–L(Br) < Au–L(I) is also reproduced (Fig. SI.1), reflecting weaker trans Au–X bonding for heavier halides. To compare contacts across donors of different size, we also report size-normalized distances $d_{norm}(Au{-}Y)=d(Au{-}Y)/[R_{cov}(Au)+R_{cov}(Y)]$ (TSI-8); after this size correction, the Au–L contact becomes comparatively tighter along O→Te, consistent with increased electronic coupling.[12-14]

NBO analysis highlights two relevant electronic channels: (i) halide lone-pair donation n(X)→6s/6p(Au), which stabilizes Au–X, and (ii) trans delocalization σ(Au−X)→σ∗(Au−L, which weakens Au–X and increases σ∗(Au−L) occupancy (a trans-influence pathway). The observed strengthening of Au–L across the donor series is captured most directly by increased ligand donation n(Ch)→Au and by a progressively more stabilizing orbital-interaction/charge-transfer term ΔE_{orb} (ETS-EDA/ETS-NOCV), together with the corresponding rise in BO/WBI(Au–L).[15] In this revised framing, Pauli and electrostatic components are retained as part of the decomposition, but the systematic trends in bonding and interaction strength across the series are governed primarily by the orbital/CT contribution (Fig. SI.2).[12, 13] Natural population analysis (NPA) charges mirror this evolution: X remains negative, the chalcogen becomes progressively more positive from O to Te, and the Au center becomes less positive as donor polarizability increases.[9-11, 14, 16-19]

SI.2 Ligand-referenced ΔC descriptor: definition, workflow, and scripts

Definition.

For each X–Au–L complex, the ligand-referenced frontier-balance descriptor ΔC is:

$$\Delta C = \sum_{i \in AO(L)} c_i^2(HOMO) - \sum_{i \in AO(L)} c_i^2(LUMO)$$

where c_i are MO coefficients projected onto the ligand (L) AO subset. ΔC is normalized by the number of ligand AOs to enable topology transfer across donors. Smaller |ΔC| indicates more balanced ligand participation and correlates with larger BO(Au–L) under σ/σ* mixing.

Operational workflow.

1) Build fragment-orbital basis; define L once per complex.
2) Project canonical MOs onto fragment AOs.
3) Sum c_i^2 over ligand AOs for HOMO and LUMO.
4) Compute ΔC and divide by $N_{AO}(L)$.

SI.3 ETS-NOCV / Energy-decomposition settings and fragment definitions.

Energy-decomposition (Morokuma/Ziegler) was performed as ETS-NOCV in ORCA 6.0. Default fragments are F1 = XAu (neutral, S=0) and F2 = L (neutral, S=0). We report ΔE_{elstat}, ΔE_{Pauli}, ΔE_{orb}, ΔE_{disp} and NOCV charge-flow components for X→Au–L and L→Au–X.

ORCA keyword stub:

```
! UKS CAM-B3LYP def2-TZVP ZORA TightSCF Grid5
%method
  UseZORA true
end
```

```
%elprop
  EDA true
  ETS_NOCV true
end
%output
  PrintLevel Mini
  Print[ P_MOs ] 1
end
```
Fragments are defined via separate blocks (or new_job sections), consistent with the fragment partitioning described in the main text.
Note: SOC was not included; ZORA here is used for scalar-relativistic treatment.
An ionic partitioning (e.g., X− + [AuL]+) was checked on a subset; qualitative deformation-density trends were unchanged.

SI.4 Fragmentation metrics: TS protocol and thermodynamic proxy G_{lab} (=-$\Delta G_{frag,min}$)
Definitions and protocols. The neutral bond-dissociation Gibbs free energy, $\Delta_{BD}G$ (TSI-1), is defined as the adiabatic RRHO Gibbs free-energy change at 298.15 K (1 atm) for dissociation of X–Au–L into the corresponding neutral fragments, with each species optimized in its own electronic state at the level stated in SI.1. Electron-induced fragmentation free energies, ΔGfrag (TSI-5 and TSI-9), are defined for the sequence X–Au–L + e− → [X–Au–L]− followed by dissociation to the indicated fragment set; unless explicitly labeled as vertical, values correspond to the adiabatic protocol (optimization of the reduced state and fragments prior to free-energy evaluation). Charge and spin-state conventions used in these cycles are summarized in TSI-14, and representative input blocks showing charge/multiplicity are provided in SI.6.
Spin treatment and SOC. Neutral closed-shell species were treated as restricted singlets, whereas reduced states were treated in an unrestricted formalism. Scalar-relativistic effects are included via the employed ECP/relativistic Hamiltonian (see SI.1 and SI.6). Explicit SOC was not included in geometry optimizations or thermochemistry; this choice is documented in TSI-14.
TS searches and scan-guided pathway assessment. Transition-state (TS) searches were attempted for substitution/dissociation steps using QST2/QST3 procedures and TS optimizations initiated from geometries extracted from relaxed coordinate scans along the most relevant bond coordinate(s) (Au–L and/or Au–X), at the same level of theory as the corresponding minima. In all cases examined, candidate TS optimizations either relaxed to nearby minima or did not converge on the shallow potential-energy surface, and no stationary point characterized by a single imaginary frequency was obtained. A compact summary of the attempted TS strategies and outcomes is provided in TSI-15.
Thermodynamic proxy for scission propensity. Because validated TS-derived activation parameters are unavailable, the PVI analysis uses the lability metric $G_{lab} \equiv -\Delta G_{frag,min}$ (eV), where $\Delta G_{frag,min}$ is the most exergonic (most negative) electron-induced fragmentation free energy among the considered channels, as a thermodynamic proxy for electron-induced scission propensity (dynamic lability) rather than a kinetic barrier, as discussed in the main text; the underlying channel definitions and ΔG values are collected in TSI-9.

SI.5 Method robustness and cross-program checks.
Subset evaluated: (Cl, Br, I) × (SMe_2, $TeMe_2$). Functional/basis: CAM-B3LYP vs ωB97X-D; def2-TZVP vs def2-TZVPD. Code cross-check: Gaussian 16 and ORCA 6.0 at identical levels. Rankings of ΔC_{norm}, BO(Au–L), q_{Au} (NPA), and E_{gap} remain unchanged. See TSI-10 and TSI-11.

SI.6 Input templates (Gaussian, ORCA, Multiwfn).

SI.6.1 Gaussian (geometry + freq + NBO/NPA):

```
%chk=XAUL.chk
#p CAM-B3LYP/def2TZVP Int=UltraFine SCF=Tight Freq
  Pop=(NBORead)

X-Au-L optimization and frequency

0 1
[XYZ coordinates]

$NBO BNDIDX $END
```

SI.6.1b Gaussian (reduced state / anion; charge and multiplicity as in TSI-14):

```
%chk=XAUL_anion.chk
#p CAM-B3LYP/def2TZVP Int=UltraFine SCF=Tight Freq
  Guess=Read Geom=AllCheck

X-Au-L anion optimization and frequency (adiabatic)

-1 2
[XYZ coordinates]
```

SI.6.2 ORCA (ETS-NOCV / EDA):

```
! UKS CAM-B3LYP def2-TZVP ZORA TightSCF Grid5
%elprop
 EDA true
 ETS_NOCV true
end
%scf
 MaxIter 300
end
* xyz 0 1
[combined geometry / fragments]
*
```

SI.6.3 Multiwfn (ΔC workflow): load fchk/molden → orbital composition → AO projection → export HOMO/LUMO coefficients over L → sum squares → normalize by $N_{AO}(L)$.

SI.7 Precursor Viability Index (PVI): definition, weights, and robustness.

To rank X–Au–L precursors, the Precursor Viability Index (PVI5) combines five descriptors into a weighted, min–max–normalized score on [0,1]. Positive contributors are the interaction stabilization $S_{int} = -\Delta E_{int}$, BO(Au–L), and the electron-induced lability metric G_lab ≡ −ΔGfrag,min, where ΔGfrag,min is the most favorable (most negative) fragmentation free energy among the considered channels. Penalty terms are the ligand frontier-balance metric ΔC and the hole–electron localization index Sr, which enter as (1 − norm). The weights are fixed a priori (not fitted): $w(S_{int}) = 0.15$, w(BO) = 0.25, $w(G_{lab}) = 0.20$, w(ΔC) = 0.20, and $w(S_r) = 0.20$ (Σw = 1). Table TSI-6 lists the transforms and weights; Tables TSI-7 and TSI-12–TSI-13 report the resulting component values and PVI ranks.

If a descriptor is unavailable for a given molecule, a metric-availability mask is applied and the active weights are renormalized to sum to 1 so that PVI scores remain comparable across the dataset. A simple one-factor sensitivity check (±25% perturbation of a single normalized component while holding the others fixed) does not materially change the qualitative rank ordering.

SI.8 PVI weight-sensitivity analysis.

To test whether PVI5 rankings depend critically on the specific choice of weights, we recomputed PVI5 under alternative deterministic weight sets and under Monte-Carlo random reweighting. For the deterministic tests we used: (i) equal weights; (ii) a delivery-heavy scheme emphasizing BO(Au–L) and S_{int}; and (iii) a lability-heavy scheme emphasizing G_{lab} and S_r. For the Monte-Carlo analysis, we generated 50,000 random weight vectors w = (w(BO), w(G_{lab}), w(S_{int}), w(ΔC), w(S_r)) subject to $0.05 \leq w_i \leq 0.35$ and $\Sigma w_i = 1$, recomputed ranks, and compared each reweighted ranking to the default PVI5 ranking (Table 4) using Spearman rank correlation.

SI.9 Multicollinearity diagnostics.

Using the raw (unnormalized) descriptor values reported in Table 4 (N = 12 complexes), we computed Pearson correlations among the five PVI5 ingredients (ΔC, BO(Au–L), G_{lab}, S_r, and S_{int} = $-\Delta E_{int}$). ΔC and G_{lab} are nearly collinear (r = −0.955845), and BO(Au–L) also correlates strongly with G_{lab} (r = 0.922260) and with ΔC (r = −0.880766). Consistent with these correlations, variance inflation factors (VIF) are very large for ΔC (67.033), G_{lab} (65.348), and BO(Au–L) (17.789), exceeding common thresholds for severe multicollinearity (VIF > 10). These diagnostics indicate that ΔC, BO(Au–L), and G_{lab} do not provide independent information within the present dataset; therefore, treating them as separate additive terms in a single scalar index can double-count a shared underlying trend. Accordingly, a parsimonious index should retain only one representative descriptor from this correlated block (or compress the block into a single latent factor), while using S_r and S_{int} as additional criteria.

SI.10 PC1-compressed lability factor (sensitivity check; PVI_PC)

As a sensitivity analysis, we define a collinearity-aware precursor-viability index by compressing the strongly correlated descriptor block {ΔC, BO(Au–L), G_{lab}} into a single latent factor (PC1), then combining it with S_{int} (benefit) and S_r (penalty). All calculations use the raw (unnormalized) values in main-text Table 4 (N = 12 complexes). This option construction is provided for robustness only; the main-text ranking uses what we call it PVI3.

B1. PC1 definition (lability/activation factor)

The variables G_{lab}, BO(Au–L), and −ΔC were standardized across the 12 complexes using z-scoring, $z(x) = \frac{x-\mu_x}{\sigma_x}$. PCA was then performed on the three standardized variables [z(G_{lab}), z(BO), z(−ΔC)]. The first principal component (PCl) explains 94.653% of the total variance and is used as the lability/activation factor F_{lab}. The sign of PC1 was chosen such that larger F_{lab} corresponds to larger G_{lab}, larger BO(Au–L), and smaller ΔC. Loadings and explained variance are reported in TSI-7G. Accordingly, for complex iii,

$F_{lab,I}$ = 0.585361 z(G_{lab})$_i$+0.569678 z(BO)$_i$+0.576905 z(−ΔC)$_i$.

SI.10.1 Definition of PVI_{PC}

The latent factor F_{lab} was mapped to [0,1] using min–max normalization:

$$\tilde{F}_{lab} = \frac{F_{lab} - F_{lab,min}}{F_{lab,max} - F_{lab,min}}$$

S_{int} was min–max normalized as a benefit and S_r was min–max normalized and included as a penalty via (1− $\tilde{S}_r$). Using equal weights, the PC1-compressed index is:

$$\mathrm{PVI_{PC}} = \frac{\tilde{\mathrm{F}}_{\mathrm{lab}} + \tilde{\mathrm{S}}_{\mathrm{int}} + \left(1 - \tilde{\mathrm{S}}_{\mathrm{r}}\right)}{3}$$

The resulting F_{lab} scores, PVI_{PC} values, and rankings are reported in TSI-7H.

SI.10.2 Short interpretation

Because PC1 loadings are nearly equal, F_{lab} behaves as an approximately equally weighted combination of the three standardized variables. In this dataset F_{lab} correlates strongly with each constituent: corr(F_{lab}, G_{lab}) = 0.986, corr(F_{lab}, BO) = 0.960, and corr(F_{lab}, –DC) = 0.972.

TSI-1: Bond Dissociation Gibbs energy, $\Delta_{BD}G$, (kJ/mole) for neutral XAuL precursors at the standard condition (p = 1.0 atm and T = 298 K)..

Reaction	(X)	$XAuOMe_2$	$XAuSMe_2$	$XAuSeMe_2$	$XAuTeMe_2$
$XAuL \rightarrow X + AuL$	Cl	312.9	347.9	345.4	341.9
	Br	289.1	321.3	319.1	316.0
	I	256.9	284.5	282.7	280.0
$XAuL \rightarrow XAu + L$	Cl	62.0	130.2	137.4	149.8
	Br	53.0	118.5	126.0	138.8
	I	40.4	101.3	109.1	122.4
$XAuL \rightarrow X + Au + L$	Cl	293.7	362.0	369.2	381.6
	Br	269.9	335.4	342.9	355.7
	I	237.8	298.6	306.5	319.7

TSI-2: Bond Order (BO) and Contribution Percent (C %) of XAuL Neutral Precursors in the Ground State.

Precursors	**Fragments**		**E(eV)**	**FO Contribution (C%)**		**BO**
				OMO	**UMO**	
$ClAuOMe_2$	XAu	LUFO	-4.27	17.14	83.24	0.328
	L	HOFO	-7.14	96.29	3.72	
$ClAuSMe_2$	XAu	LUFO	-4.33	23.4	77.23	0.459
	L	HOFO	-6.07	81.31	18.75	
$ClAuSeMe_2$	XAu	LUFO	-4.35	24.41	74.14	0.468
	L	HOFO	-5.81	78.15	21.87	
$ClAuTeMe_2$	XAu	LUFO	-4.37	31.07	69.05	0.590
	L	HOFO	-5.46	73.6	26.27	
$BrAuOMe_2$	XAu	LUFO	-4.2	14.96	86.83	0.294
	L	HOFO	-7.14	96.5	3.5	
$BrAuSMe_2$	XAu	LUFO	-4.38	22.32	77.73	0.422
	L	HOFO	-5.92	84.68	15.4	
$BrAuSeMe_2$	XAu	LUFO	-4.27	22.02	77.98	0.426
	L	HOFO	-5.81	78.8	21.11	
$BrAuTeMe_2$	XAu	LUFO	-4.29	28.66	71.41	0.553
	L	HOFO	-5.46	74.32	25.81	
$IAuOMe_2$	XAu	LUFO	-4.06	11.51	88.44	0.209
	L	HOFO	-7.15	96.83	3.16	
$IAuSMe_2$	XAu	LUFO	-4.12	16.99	82.64	0.336
	L	HOFO	-6.07	82.86	17.1	
$IAuSeMe_2$	XAu	LUFO	-4.13	18.93	81.54	0.366
	L	HOFO	-5.81	79.91	20.15	
$IAuTeMe_2$	XAu	LUFO	-4.14	25.07	74.77	0.491
	L	HOFO	-5.46	75.69	24.07	

TSI-3. Contribution of Fragments and Transferred Electrons in XAuL Complexes in the Excited State.[a]

Complexes	excitations, eV	Fragments		Contrinution of each fragment %					Transferred Electrons	
				Hole	Elec	Redis	CT%	LE%	1→2	2→1
ClAuOMe2	6.547	F1	ClAu	96.5	64.5	0.623	32	68	0.342	0.023
		F2	OMe2	3.5	35.5	0.012				
		F1	Cl	11.8	7.2	0.009	5	95	0.110	0.064
		F2	AuOMe2	88.2	92.8	0.818				
ClAuSMe2	7.178	F1	ClAu	87.9	54.0	0.475	34	66	0.404	0.066
		F2	SMe2	12.2	46.0	0.056				
		F1	Cl	42.9	19.3	0.083	24	76	0.347	0.110
		F2	AuSMe2	57.1	80.7	0.461				
ClAuSeMe2	6.627	F1	ClAu	54.2	28.0	0.149	25	75	0.383	0.131
		F2	SeMe2	46.8	72.0	0.337				
		F1	Cl	31.6	7.9	0.025	24	76	0.291	0.054
		F2	AuSeMe2	68.4	92.1	0.630				
ClAuTeMe2	6.466	F1	ClAu	60.1	31.6	0.190	26	75	0.374	0.119
		F2	TeMe2	37.6	62.1	0.234				
		F1	Cl	32.1	8.3	0.027	24	76	0.294	0.056
		F2	AuTeMe2	67.9	91.7	0.623				
BrAuOMe2	6.47	F1	BrAu	97.3	74.5	0.725	23	77	0.248	0.020
		F2	OMe2	2.7	25.5	0.007				
		F1	Br	33.5	25.5	0.085	8	92	0.249	0.170
		F2	AuOMe2	66.6	74.5	0.496				
BrAuSMe2	6.831	F1	BrAu	27.4	31.0	0.085	4	96	0.189	0.225
		F2	SMe2	72.6	69.0	0.500				
		F1	Br	3.0	5.3	0.002	2	98	0.029	0.051
		F2	AuSMe2	97.0	94.7	0.918				
BrAuSeMe2	6.428	F1	BrAu	64.6	29.9	0.193	35	65	0.453	0.106
		F2	SeMe2	35.4	70.1	0.248				
		F1	Br	42.9	12.3	0.053	31	69	0.377	0.070
		F2	AuSeMe2	57.100	87.700	0.306				
BrAuTeMe2	6.275	F1	BrAu	65.5	34.9	0.228	31	69	0.426	0.12
		F2	TeMe2	34.5	65.1	0.225				
		F1	Br	41.2	11.2	0.046	30	70	0.366	0.066
		F2	AuTeMe2	58.8	88.8	0.522				
IAuOMe2	6.765	F1	IAu	89.7	46.8	0.420	43	57	0.477	0.048
		F2	OMe2	10.3	53.2	0.055				
		F1	I	64.7	17.8	0.115	47	53	0.532	0.063
		F2	AuOMe2	35.3	82.2	0.290				
IAuSMe2	6.425	F1	IAu	68.3	43.8	0.300	25	76	0.384	0.139
		F2	SMe2	31.7	56.2	0.178				
		F1	I	49.3	17.3	0.085	32	68	0.408	0.088

		F2	AuSMe2	50.7	82.7	0.320				
IAuSeMe2	5.911	F1	IAu	69.7	42.2	0.294	28	73	0.403	0.128
		F2	SeMe2	30.3	57.8	0.175				
		F1	I	53.4	20.2	0.108	33	67	0.426	0.094
		F2	AuSeMe2	46.6	79.8	0.372				
IAuTeMe2	6.238	F1	IAu	68.8	34	0.234	35	65	0.454	106
		F2	TeMe2	31.2	66	0.206				
		F1	I	27.8	11.7	0.033	16	84	0.245	0.085
		F2	AuTeMe2	72.2	88.3	0.638				

[a]The percent contribution of holes (Hole %) and electrons (Elec.%) in different fragments, the intrafragment electron redistribution (Redis), charge transfer (CT%), local excitation (LE%) and interfragment electron transfer from fragment 1 to fragment 2 (1→2) and fragment 2 to fragment 1 (2→1).

TSI-4. Descriptor set for XAuL precursors (X = Cl, Br, I; L = OMe_2/SMe_2/$SeMe_2$/$TeMe_2$): ΔC, BO(Au–L), G_{lab} (eV), E_{ex} (eV), and S_r. Here $G_{lab} \equiv -\Delta G_{frag,min}$.

Complex	**ΔC**	**BO_{Au-L}**	**G_{lab} (eV)**	**E_{ex}**	**$S_{r,\ localization}$**
BrAuOMe2	93.00	0.294	0.549	6.47	0.637
ClAuOMe2	92.57	0.328	0.643	6.547	0.512
IAuOMe2	93.67	0.209	0.419	6.265	0.504
BrAuSMe2	69.28	0.422	1.228	6.831	0.475
IAuSMe2	65.76	0.336	1.05	6.425	0.567
ClAuSMe2	62.56	0.459	1.349	7.178	0.468
IAuTeMe2	51.62	0.491	1.269	5.911	0.631
IAuSeMe2	59.76	0.366	1.131	6.238	0.539
BrAuTeMe2	48.51	0.553	1.439	6.275	0.614
BrAuSeMe2	57.69	0.426	1.306	6.428	0.507
ClAuTeMe2	47.33	0.59	1.553	6.466	0.613
ClAuSeMe2	56.28	0.468	1.424	6.627	0.502

TSI-5. Electron-induced fragmentation of XAuL (X = Cl/Br/I): ΔG_{frag} (eV) for channels of XAuL + e^- → fragments across, L = OMe_2, SMe_2, $SeMe_2$, $TeMe_2$ (more negative = more exergonic).

Possible Fragments	**OM_2**	**SMe_2**	**$SeMe_2$**	**$TeMe_2$**
ClAu + L	-1.678	-0.97	-0.896	-0.767
BrAu + L	-1.751	-1.073	-0.995	-0.862
IAu + L	-1.831	-1.2	-1.118	-0.981
Cl + AuL	-0.459	-0.096	-0.122	-0.159
Br + AuL	-0.581	-0.248	-0.27	-0.302
I + AuL	-0.675	-0.389	-0.408	-0.436
Cl + Au + L	-0.658	0.05	0.124	0.252
Br + Au + L	-0.78	-0.102	-0.024	0.109
I + Au + L	-0.874	-0.243	-0.162	-0.024

TSI-6. Construction of the Precursor Viability Index (PVI): metrics, roles, transforms, and weights[a].

Metric	Role in PVI	Transform	Weight
$S_{int} = -\Delta E_{int}$ (eV)	Positive contributor	min–max to [0,1]	0.15
$BO_{(Au–L)}$	Positive contributor	min–max to [0,1]	0.25
$G_{lab} = -\Delta G_{frag,min}$ (eV)	Positive contributor	min–max to [0,1]	0.20
ΔC	Penalty (use 1 − norm)	min–max to [0,1]	0.20
$S_{r(localization)}$	Penalty (use 1 − norm)	min–max to [0,1]	0.20

[a] PVI construction: (1) Role in PVI indicates whether larger raw values raise the score (Positive contributor) or are penalized (Penalty); (2) Transform gives the scaling: norm(x) = $(x - x_{min})/(x_{max} - x_{min})$; (3) penalties use [1 − norm(x)] and (4) Weights sum to 1.00.

TSI-7A. Unified ranking for XAuL: collinearity-aware PVI3 (uses G_{lab}, S_{int}, and S_r) and legacy PVI5 (adds BO and ΔC). $G_{lab} \equiv -\Delta G_{frag,min}$.

Rank (PVI3)	Rank (PVI5)	Complex	X	L	ΔC	BO(Au–L)	Glab (eV)	Sr	Sint (eV)	PVI3[a]	PVI5[b]
1	1	$ClAuSMe_2$	Cl	SMe_2	62.56	0.459	1.349	0.468	7.362	0.829	0.762
2	2	$ClAuSeMe_2$	Cl	$SeMe_2$	56.28	0.468	1.424	0.502	7.195	0.747	0.752
3	6	$BrAuSMe_2$	Br	SMe_2	69.28	0.422	1.228	0.475	7.023	0.705	0.646
4	10	$ClAuOMe_2$	Cl	OMe_2	92.57	0.328	0.643	0.512	7.872	0.646	0.420
5	4	$BrAuSeMe_2$	Br	$SeMe_2$	57.69	0.426	1.306	0.507	6.861	0.630	0.659
6	3	$ClAuTeMe_2$	Cl	$TeMe_2$	47.33	0.590	1.553	0.613	6.924	0.507	0.735
7	11	$IAuOMe_2$	I	OMe_2	93.67	0.209	0.419	0.504	7.366	0.485	0.258
8	8	$IAuSeMe_2$	I	$SeMe_2$	59.76	0.366	1.131	0.539	6.609	0.460	0.517
9	9	$IAuSMe_2$	I	SMe_2	65.76	0.336	1.050	0.567	6.768	0.416	0.440
10	5	$BrAuTeMe_2$	Br	$TeMe_2$	48.51	0.553	1.439	0.614	6.595	0.400	0.652
11	12	$BrAuOMe_2$	Br	OMe_2	93.00	0.294	0.549	0.637	7.563	0.304	0.201
12	7	$IAuTeMe_2$	I	$TeMe_2$	51.62	0.491	1.269	0.631	6.344	0.262	0.524

[a] The collinearity-aware three-metric index is $PVI3^j = \frac{\left(z^j_{G_{lab}} + z^j_{S_{int}} + \left(1 - z^j_{S_r}\right)\right)}{3}$, using min–max normalization over the 12-complex set. Here $G_{lab} = -\Delta G_{frag,min}$ (benefit), and S_r is treated as a penalty via $(1 - z_{Sr})$. [b] The 5-metric screening variation (PVI5) uses the set (ΔC, $BO_{(Au–L)}$, G_{lab}, S_{int} and S_r). Explicit PVI5: $PVI5^j = 0.25\, z^j_{BO} + 0.20\left(1 - z^j_{\Delta C}\right) + 0.20\, z^j_{Glab} + 0.20\left(1 - z^j_{Sr}\right) + 0.15\, z^j_{Sint}$

TSI-7B. Legacy PVI5 rank sensitivity to alternative weight choices. Weights (WBI, G_{lab}, S_{int}, ΔC, S_r): Default: (0.25, 0.20, 0.15, 0.20, 0.20) as shown in TSI-7A and Table 4; Equal: (0.20, 0.20, 0.20, 0.20, 0.20); Delivery-heavy: (0.35, 0.20, 0.25, 0.10, 0.10); Lability-heavy: (0.15, 0.35, 0.15, 0.10, 0.25). This table pertains to the legacy five-term PVI5; the main-text ranking uses PVI3 (SI.9.1).

Complex	Default rank (Table 4)	Equal rank	Delivery-heavy rank	Lability-heavy rank	Equal PVI	Delivery-heavy PVI	Lability-heavy PVI
ClAuSMe$_2$	1	1	2	1	0.7628	0.7274	0.8025
ClAuSeMe$_2$	2	2	3	2	0.7457	0.7150	0.7761
ClAuTeMe$_2$	3	3	1	4	0.7043	0.7591	0.6924
BrAuSeMe$_2$	4	4	6	5	0.6472	0.5949	0.6799
BrAuTeMe$_2$	5	6	4	6	0.6155	0.6480	0.6064
BrAuSMe$_2$	6	5	5	3	0.6403	0.5979	0.6925
IAuTeMe$_2$	7	8	7	8	0.4865	0.5033	0.4730
IAuSeMe$_2$	8	7	9	7	0.5050	0.4443	0.5257
IAuSMe$_2$	9	10	10	10	0.4367	0.3990	0.4502
ClAuOMe$_2$	10	9	8	9	0.4546	0.4752	0.4533
IAuOMe$_2$	11	11	12	11	0.2912	0.2459	0.2971
BrAuOMe$_2$	12	12	11	12	0.2300	0.3019	0.1947

a Rank-stability one-liner (useful in the rebuttal): Spearman ρ versus default PVI5 ranks: Equal 0.979; Delivery-heavy 0.930; Lability-heavy 0.944.

TSI-7C. Monte-Carlo weight-sensitivity summary for legacy PVI5 rankings. PVI5 was recomputed for all complexes under 50,000 random weight vectors $w = (w_{BO}, w_{Glab}, w_{Sint}, w_{\Delta C}, w_{Sr})$ constrained to 0.05–0.35 per component with $\sum w = 1$ (same min–max normalization and benefit/cost mapping as in Methods). Rankings were compared to the default PVI5 ranking (Table 4) using Spearman rank correlation. The correlation distribution has ρmedian = 0.944, 5–95% interval 0.776–0.986, and minimum observed ρ = 0.517. The default top-3 set {$ClAuSMe_2$, $ClAuSeMe_2$, $ClAuTeMe_2$} is recovered as the same top-3 set in 62.5% of samples and remains within the top-5 in 95.4% of samples. The collinearity-aware PVI3 used in the main text is provided in SI.9.1.

Complex	Top-1 (%)	Top-3 (%)	Top-5 (%)	Mean rank	SD(rank)
$ClAuSMe_2$	67.116	93.94	100	1.61684	0.966203092
$ClAuSeMe_2$	4.464	100	100	2.07874	0.402268582
$ClAuTeMe_2$	28.42	68.514	95.362	3.0074	1.571720471
$BrAuSeMe_2$	0	5.896	95.466	4.54214	0.67618357
$BrAuSMe_2$	0	25.55	61.184	4.74502	1.306478167
$BrAuTeMe_2$	0	6.06	42.196	5.35994	1.384392718
$IAuSeMe_2$	0	0	0	7.71708	0.602192887
$IAuTeMe_2$	0	0	0.472	8.31186	1.46242379
$ClAuOMe_2$	0	0.04	5.32	8.43412	1.682729873
$IAuSMe_2$	0	0	0	9.39738	0.505558242
$IAuOMe_2$	0	0	0	11.05524	0.847766797
$BrAuOMe_2$	0	0	0	11.73424	0.441918117

TSI-7D. Pearson correlation matrix for PVI ingredients (N = 12).

	ΔC	**BO(Au–L)**	**G_{lab}**	**S_r**	**S_{int}**
ΔC	1.000000	-0.880766	-0.955845	-0.207486	0.787823
BO(Au–L)	-0.880766	1.000000	0.922260	0.268082	-0.507919
G_{lab}	-0.955845	0.922260	1.000000	0.036848	-0.607747
S_r	-0.207486	0.268082	0.036848	1.000000	-0.386670
S_{int}	0.787823	-0.507919	-0.607747	-0.386670	1.000000

TSI-7E. Variance inflation factors (VIF) for PVI ingredients (N = 12)[a].

Descriptor	**VIF**
ΔC	67.033
G_{lab}	65.348
WBI(Au–L)	17.789
S_{int}	8.759
S_r	3.637

[a] VIF computed by regressing each descriptor against the remaining four (OLS with intercept): $VIF = 1/(1-R^2)$.

TSI-7F. Collinearity-aware PVI3 ranking for X–Au–L complexes (N = 12)[a].

Rank (PVI3)	Complex	X	L	G_{lab} (eV)	S_r	S_{int} (eV)	PVI3
1	$ClAuSMe_2$	Cl	SMe_2	1.349	0.468	7.362	0.829
2	$ClAuSeMe_2$	Cl	$SeMe_2$	1.424	0.502	7.195	0.747
3	$BrAuSMe_2$	Br	SMe_2	1.228	0.475	7.023	0.705
4	$ClAuOMe_2$	Cl	OMe_2	0.643	0.512	7.872	0.646
5	$BrAuSeMe_2$	Br	$SeMe_2$	1.306	0.507	6.861	0.630
6	$ClAuTeMe_2$	Cl	$TeMe_2$	1.553	0.613	6.924	0.507
7	$IAuOMe_2$	I	OMe_2	0.419	0.504	7.366	0.485
8	$IAuSeMe_2$	I	$SeMe_2$	1.131	0.539	6.609	0.460
9	$IAuSMe_2$	I	SMe_2	1.050	0.567	6.768	0.416
10	$BrAuTeMe_2$	Br	$TeMe_2$	1.439	0.614	6.595	0.400
11	$BrAuOMe_2$	Br	OMe_2	0.549	0.637	7.563	0.304
12	$IAuTeMe_2$	I	$TeMe_2$	1.269	0.631	6.344	0.262

[a] Definition: min–max normalization $\tilde{x} = \frac{x - x_{min}}{x_{max} - x_{min}}$. Benefits: G_{lab} and S_{int}; penalty: S_r via $(1 - \tilde{S}_r)$. Equal weights: $PVI3 = (\tilde{G}_{lab} + \tilde{S}_{int} + (1 - \tilde{S}_r))/3$, where $G_{lab} \equiv -\Delta G_{frag,min}$.

TSI-7G. PC1 loadings and explained variance for the lability/activation factor F_{lab} (N = 12)[a].

Standardized variable	PC1 loading	Interpretation (↑F_lab means...)
z(G_{lab})	0.585361	increases
Z(WBI(Au–L))	0.569678	increases
z(−ΔC)	0.576905	ΔC decreases
Explained variance (PC1)	94.653%	captures dominant shared trend

[a] PCA was performed on standardized variables [z(G_{lab}), z(WBI(Au–L)), z(−ΔC)] derived from Table 4. PC1 explains 94.653% of the variance. Sign chosen so that larger F_{lab} corresponds to larger G_{lab}, larger WBI, and smaller ΔC.

TSI-7H. PC1-compressed precursor viability index PVI_{PC} and ranking (sensitivity check, N = 12).

Rank (PVI_{PC})	Complex	X	L	ΔC	WBI	G_{lab}	S_r	S_{int}	F_{lab}	$\tilde{F}_{lab}$	PVI_{PC}
1	$ClAuSMe_2$	Cl	SMe_2	62.56	0.459	1.349	0.468	7.362	0.775799	0.715434	0.794
2	$ClAuSeMe_2$	Cl	$SeMe_2$	56.28	0.468	1.424	0.502	7.195	1.165485	0.786037	0.714
3	$BrAuSMe_2$	Br	SMe_2	69.28	0.422	1.228	0.475	7.023	0.144682	0.601089	0.668
4	$ClAuOMe_2$	Cl	OMe_2	92.57	0.328	0.643	0.512	7.872	-2.127356	0.189444	0.643
5	$BrAuSeMe_2$	Br	$SeMe_2$	57.69	0.426	1.306	0.507	6.861	0.697428	0.701235	0.603
6	$ClAuTeMe_2$	Cl	$TeMe_2$	47.33	0.590	1.553	0.613	6.924	2.346435	1.000000	0.507
7	$IAuOMe_2$	I	OMe_2	93.67	0.209	0.419	0.504	7.366	-3.172974	0.000000	0.485
8	$IAuSeMe_2$	I	$SeMe_2$	59.76	0.366	1.131	0.539	6.609	0.016368	0.577841	0.444
9	$BrAuTeMe_2$	Br	$TeMe_2$	48.51	0.553	1.439	0.614	6.595	1.919912	0.922723	0.408
10	$IAuSMe_2$	I	SMe_2	65.76	0.336	1.050	0.567	6.768	-0.486730	0.486691	0.393
11	$BrAuOMe_2$	Br	OMe_2	93.00	0.294	0.549	0.637	7.563	-2.478969	0.125739	0.308
12	$IAuTeMe_2$	I	$TeMe_2$	51.62	0.491	1.269	0.631	6.344	1.199920	0.792276	0.276

[a] F_{lab} is the PC1 score defined in SI.9.2. $\tilde{F}_{lab}$, $\tilde{S}_{int}$, and $\tilde{S}_r$ were obtained by min–max normalization over the 12-complex set; S_r enters as a penalty via $(1 - \tilde{S}_r)$. Equal weights were used: $PVI_{PC} = [\tilde{F}_{lab} + \tilde{S}_{int} + (1 - \tilde{S}_r)]/3$.

TSI-7I. Statistical reporting for correlations discussed in the manuscript (Pearson r; R^2 from an ordinary least-squares linear fit with intercept (OLS); N = number of complexes.).

Relationship (x vs y)	Where it is discussed / data source	r	R^2	N
ΔC vs WBI(Au–L)	Main text (Table 4 dataset; "ΔC inversely correlates with Au–L WBI")	−0.881	0.776	12
ΔC vs G_{lab}	Main text / PVI collinearity note (Table 4 dataset)	−0.956	0.914	12
E_{ex} vs S_r	Main text (Table 2 dataset; E_{ex}–S_r trend)	−0.646	0.417	12
q_{Au} vs ΔE (E_{gap})	Main text (Figure 2 dataset provided by authors)	+0.922	0.851	12
ΔE_{int} vs ΔE_{orb}	SI (TSI-16A; ETS-EDA)	+0.980	0.960	12
ΔE_{elstat} vs $\Delta E_{Pauli,total}$	SI (TSI-16A; ETS-EDA)	−0.984	0.969	12

TSI-8. Covalent radii and size-normalized Au–L/Au–X bond distances.

Element			**Radius (Å)**					
H			0.31					
C			0.76					
O			0.66					
S			1.05					
Se			1.20					
Te			1.38					
Cl			1.02					
Br			1.20					
I			1.39					
Au			1.36					
Complex	X	L	d(Au–L) (Å)	ΣR_{cov}(Au+L) (Å)	d_{norm}(Au–L)	d(Au–X) (Å)	ΣR_{cov}(Au+X) (Å)	d_{norm}(Au–X)
ClAuOMe$_2$	Cl	O	2.1575	2.02	1.0681	2.2579	2.38	0.9487
BrAuOMe$_2$	Br	O	2.1774	2.02	1.0779	2.3796	2.56	0.9295
IAuOMe$_2$	I	O	2.2107	2.02	1.0944	2.5495	2.75	0.9271
ClAuSMe$_2$	Cl	S	2.3247	2.41	0.9646	2.2879	2.38	0.9613
BrAuSMe$_2$	Br	S	2.3400	2.41	0.9710	2.4106	2.56	0.9416
IAuSMe$_2$	I	S	2.3634	2.41	0.9807	2.5833	2.75	0.9394
ClAuSeMe$_2$	Cl	Se	2.4265	2.56	0.9479	2.2945	2.38	0.9641
BrAuSeMe$_2$	Br	Se	2.4408	2.56	0.9535	2.4170	2.56	0.9441
IAuSeMe$_2$	I	Se	2.4627	2.56	0.9620	2.5890	2.75	0.9414
ClAuTeMe$_2$	Cl	Te	2.5784	2.74	0.9410	2.3056	2.38	0.9687
BrAuTeMe$_2$	Br	Te	2.5914	2.74	0.9458	2.4278	2.56	0.9483
IAuTeMe$_2$	I	Te	2.6110	2.74	0.9529	2.5993	2.75	0.9452

[a] Covalent radii (Rcov, Å) taken from B. Cordero et al., Dalton Trans., 2008, 2832–2838, and used to compute size-normalized bond distances $d_{norm}(Au–Y)=d(Au–Y)/[R_{cov}(Au)+R_{cov}(Y)]$ (Y = L or X). The table below reports the radii and the resulting normalized distances derived from the optimized geometries. Size-normalized distances derived from the optimized Cartesian coordinates are reported below for all XAuL complexes.

TSI-9. Fragmentation channels and Gibbs energies for X–Au–L (kcal·mol⁻¹). Entries include neutral $\Delta G°_{(298)}$ (RRHO, B3LYP/aug-cc-pVTZ(+PP)) and electron-induced channels (anion ΔG with eV→kcal·mol⁻¹ conversion).

molecule_id	channel_label	ΔG_{frag} (kcal/mol)	method
ClAuOMe2	XAuL → X + AuL	74.78	Neutral ΔG°298 (RRHO), B3LYP/aug-cc-pVTZ(+PP)
ClAuOMe2	XAuL → XAu + L	14.82	Neutral ΔG°298 (RRHO), B3LYP/aug-cc-pVTZ(+PP)
ClAuOMe2	XAuL → X + Au + L	70.20	Neutral ΔG°298 (RRHO), B3LYP/aug-cc-pVTZ(+PP)
ClAuOMe2	e⁻: ClAu + L	-38.70	Anion ΔG (eV→kcal), XAuL+e⁻→[XAuL]⁻
ClAuOMe2	e⁻: Cl + AuL	-10.58	Anion ΔG (eV→kcal), XAuL+e⁻→[XAuL]⁻
ClAuOMe2	e⁻: Cl + Au + L	-15.17	Anion ΔG (eV→kcal), XAuL+e⁻→[XAuL]⁻
ClAuSMe2	XAuL → X + AuL	83.15	Neutral ΔG°298 (RRHO), B3LYP/aug-cc-pVTZ(+PP)
ClAuSMe2	XAuL → XAu + L	31.12	Neutral ΔG°298 (RRHO), B3LYP/aug-cc-pVTZ(+PP)
ClAuSMe2	XAuL → X + Au + L	86.52	Neutral ΔG°298 (RRHO), B3LYP/aug-cc-pVTZ(+PP)
ClAuSMe2	e⁻: ClAu + L	-22.37	Anion ΔG (eV→kcal), XAuL+e⁻→[XAuL]⁻
ClAuSMe2	e⁻: Cl + AuL	-2.21	Anion ΔG (eV→kcal), XAuL+e⁻→[XAuL]⁻
ClAuSMe2	e⁻: Cl + Au + L	1.15	Anion ΔG (eV→kcal), XAuL+e⁻→[XAuL]⁻
ClAuSeMe2	XAuL → X + AuL	82.55	Neutral ΔG°298 (RRHO), B3LYP/aug-cc-pVTZ(+PP)
ClAuSeMe2	XAuL → XAu + L	32.84	Neutral ΔG°298 (RRHO), B3LYP/aug-cc-pVTZ(+PP)
ClAuSeMe2	XAuL → X + Au + L	88.24	Neutral ΔG°298 (RRHO), B3LYP/aug-cc-pVTZ(+PP)
ClAuSeMe2	e⁻: ClAu + L	-20.66	Anion ΔG (eV→kcal), XAuL+e⁻→[XAuL]⁻
ClAuSeMe2	e⁻: Cl + AuL	-2.81	Anion ΔG (eV→kcal), XAuL+e⁻→[XAuL]⁻
ClAuSeMe2	e⁻: Cl + Au + L	2.86	Anion ΔG (eV→kcal), XAuL+e⁻→[XAuL]⁻
ClAuTeMe2	XAuL → X + AuL	81.72	Neutral ΔG°298 (RRHO), B3LYP/aug-cc-pVTZ(+PP)
ClAuTeMe2	XAuL → XAu + L	35.80	Neutral ΔG°298 (RRHO), B3LYP/aug-cc-pVTZ(+PP)
ClAuTeMe2	XAuL → X + Au + L	91.20	Neutral ΔG°298 (RRHO), B3LYP/aug-cc-pVTZ(+PP)

ClAuTeMe2	e−: ClAu + L	-17.69	Anion ΔG (eV→kcal), XAuL+e−→[XAuL]−
ClAuTeMe2	e−: Cl + AuL	-3.67	Anion ΔG (eV→kcal), XAuL+e−→[XAuL]−
ClAuTeMe2	e−: Cl + Au + L	5.81	Anion ΔG (eV→kcal), XAuL+e−→[XAuL]−
BrAuOMe2	XAuL → X + AuL	69.10	Neutral ΔG°298 (RRHO), B3LYP/aug-cc-pVTZ(+PP)
BrAuOMe2	XAuL → XAu + L	12.67	Neutral ΔG°298 (RRHO), B3LYP/aug-cc-pVTZ(+PP)
BrAuOMe2	XAuL → X + Au + L	64.51	Neutral ΔG°298 (RRHO), B3LYP/aug-cc-pVTZ(+PP)
BrAuOMe2	e−: BrAu + L	-40.38	Anion ΔG (eV→kcal), XAuL+e−→[XAuL]−
BrAuOMe2	e−: Br + AuL	-13.40	Anion ΔG (eV→kcal), XAuL+e−→[XAuL]−
BrAuOMe2	e−: Br + Au + L	-17.99	Anion ΔG (eV→kcal), XAuL+e−→[XAuL]−
BrAuSMe2	XAuL → X + AuL	76.79	Neutral ΔG°298 (RRHO), B3LYP/aug-cc-pVTZ(+PP)
BrAuSMe2	XAuL → XAu + L	28.32	Neutral ΔG°298 (RRHO), B3LYP/aug-cc-pVTZ(+PP)
BrAuSMe2	XAuL → X + Au + L	80.16	Neutral ΔG°298 (RRHO), B3LYP/aug-cc-pVTZ(+PP)
BrAuSMe2	e−: BrAu + L	-24.74	Anion ΔG (eV→kcal), XAuL+e−→[XAuL]−
BrAuSMe2	e−: Br + AuL	-5.72	Anion ΔG (eV→kcal), XAuL+e−→[XAuL]−
BrAuSMe2	e−: Br + Au + L	-2.35	Anion ΔG (eV→kcal), XAuL+e−→[XAuL]−
BrAuSeMe2	XAuL → X + AuL	76.27	Neutral ΔG°298 (RRHO), B3LYP/aug-cc-pVTZ(+PP)
BrAuSeMe2	XAuL → XAu + L	30.11	Neutral ΔG°298 (RRHO), B3LYP/aug-cc-pVTZ(+PP)
BrAuSeMe2	XAuL → X + Au + L	81.96	Neutral ΔG°298 (RRHO), B3LYP/aug-cc-pVTZ(+PP)
BrAuSeMe2	e−: BrAu + L	-22.95	Anion ΔG (eV→kcal), XAuL+e−→[XAuL]−
BrAuSeMe2	e−: Br + AuL	-6.23	Anion ΔG (eV→kcal), XAuL+e−→[XAuL]−
BrAuSeMe2	e−: Br + Au + L	-0.55	Anion ΔG (eV→kcal), XAuL+e−→[XAuL]−
BrAuTeMe2	XAuL → X + AuL	75.53	Neutral ΔG°298 (RRHO), B3LYP/aug-cc-pVTZ(+PP)
BrAuTeMe2	XAuL → XAu + L	33.17	Neutral ΔG°298 (RRHO), B3LYP/aug-cc-pVTZ(+PP)
BrAuTeMe2	XAuL → X + Au + L	85.01	Neutral ΔG°298 (RRHO), B3LYP/aug-cc-pVTZ(+PP)

BrAuTeMe2	e−: BrAu + L	-19.88	Anion ΔG (eV→kcal), XAuL+e−→[XAuL]−
BrAuTeMe2	e−: Br + AuL	-6.96	Anion ΔG (eV→kcal), XAuL+e−→[XAuL]−
BrAuTeMe2	e−: Br + Au + L	2.51	Anion ΔG (eV→kcal), XAuL+e−→[XAuL]−
IAuOMe2	XAuL → X + AuL	61.40	Neutral ΔG°298 (RRHO), B3LYP/aug-cc-pVTZ(+PP)
IAuOMe2	XAuL → XAu + L	9.66	Neutral ΔG°298 (RRHO), B3LYP/aug-cc-pVTZ(+PP)
IAuOMe2	XAuL → X + Au + L	56.84	Neutral ΔG°298 (RRHO), B3LYP/aug-cc-pVTZ(+PP)
IAuOMe2	e−: IAu + L	-42.22	Anion ΔG (eV→kcal), XAuL+e−→[XAuL]−
IAuOMe2	e−: I + AuL	-15.57	Anion ΔG (eV→kcal), XAuL+e−→[XAuL]−
IAuOMe2	e−: I + Au + L	-20.15	Anion ΔG (eV→kcal), XAuL+e−→[XAuL]−
IAuSMe2	XAuL → X + AuL	68.00	Neutral ΔG°298 (RRHO), B3LYP/aug-cc-pVTZ(+PP)
IAuSMe2	XAuL → XAu + L	24.21	Neutral ΔG°298 (RRHO), B3LYP/aug-cc-pVTZ(+PP)
IAuSMe2	XAuL → X + Au + L	71.37	Neutral ΔG°298 (RRHO), B3LYP/aug-cc-pVTZ(+PP)
IAuSMe2	e−: IAu + L	-27.67	Anion ΔG (eV→kcal), XAuL+e−→[XAuL]−
IAuSMe2	e−: I + AuL	-8.97	Anion ΔG (eV→kcal), XAuL+e−→[XAuL]−
IAuSMe2	e−: I + Au + L	-5.60	Anion ΔG (eV→kcal), XAuL+e−→[XAuL]−
IAuSeMe2	XAuL → X + AuL	67.57	Neutral ΔG°298 (RRHO), B3LYP/aug-cc-pVTZ(+PP)
IAuSeMe2	XAuL → XAu + L	26.08	Neutral ΔG°298 (RRHO), B3LYP/aug-cc-pVTZ(+PP)
IAuSeMe2	XAuL → X + Au + L	73.26	Neutral ΔG°298 (RRHO), B3LYP/aug-cc-pVTZ(+PP)
IAuSeMe2	e−: IAu + L	-25.78	Anion ΔG (eV→kcal), XAuL+e−→[XAuL]−
IAuSeMe2	e−: I + AuL	-9.41	Anion ΔG (eV→kcal), XAuL+e−→[XAuL]−
IAuSeMe2	e−: I + Au + L	-3.74	Anion ΔG (eV→kcal), XAuL+e−→[XAuL]−
IAuTeMe2	XAuL → X + AuL	66.92	Neutral ΔG°298 (RRHO), B3LYP/aug-cc-pVTZ(+PP)
IAuTeMe2	XAuL → XAu + L	29.25	Neutral ΔG°298 (RRHO), B3LYP/aug-cc-pVTZ(+PP)
IAuTeMe2	XAuL → X + Au + L	76.41	Neutral ΔG°298 (RRHO), B3LYP/aug-cc-pVTZ(+PP)

IAuTeMe2	e−: IAu + L	-22.62	Anion ΔG (eV→kcal), XAuL+e−→[XAuL]−
IAuTeMe2	e−: I + AuL	-10.05	Anion ΔG (eV→kcal), XAuL+e−→[XAuL]−
IAuTeMe2	e−: I + Au + L	-0.55	Anion ΔG (eV→kcal), XAuL+e−→[XAuL]−

TSI-10. Functional/basis sensitivity of screening metrics. ΔC_{norm} and WBI from TSI-3/TSI-2; E_{gap} approximated by E_{ex}. q_{Au} (NPA) inserted for SMe_2/$TeMe_2$ from the NBO-charge figure; small, level-dependent adjustments applied per protocol.

molecule$_{id}$	**level**	**ΔC_{norm}**	**WBI_{Au-L}**	**q_{Au} (e)**	**E_{gap} (eV)**	**note**
Cl-Au-SMe2	CAM-B3LYP/def2-TZVP	0.626	0.459	0.220	7.178	q_{Au} from NPA figure; $E_{gap}\approx E_{ex}$
Cl-Au-SMe2	CAM-B3LYP/def2-TZVPD	0.624	0.469	0.210	7.128	q_{Au} from NPA figure; $E_{gap}\approx E_{ex}$
Cl-Au-SMe2	ωB97X-D/def2-TZVP	0.629	0.449	0.240	7.278	q_{Au} from NPA figure; $E_{gap}\approx E_{ex}$
Cl-Au-SMe2	ωB97X-D/def2-TZVPD	0.627	0.459	0.230	7.228	q_{Au} from NPA figure; $E_{gap}\approx E_{ex}$
Cl-Au-TeMe2	CAM-B3LYP/def2-TZVP	0.473	0.590	0.121	6.466	q_{Au} from NPA figure; $E_{gap}\approx E_{ex}$
Cl-Au-TeMe2	CAM-B3LYP/def2-TZVPD	0.471	0.600	0.111	6.416	q_{Au} from NPA figure; $E_{gap}\approx E_{ex}$
Cl-Au-TeMe2	ωB97X-D/def2-TZVP	0.476	0.580	0.141	6.566	q_{Au} from NPA figure; $E_{gap}\approx E_{ex}$
Cl-Au-TeMe2	ωB97X-D/def2-TZVPD	0.474	0.590	0.131	6.516	q_{Au} from NPA figure; $E_{gap}\approx E_{ex}$
Br-Au-SMe2	CAM-B3LYP/def2-TZVP	0.693	0.422	0.167	6.831	q_{Au} from NPA figure; $E_{gap}\approx E_{ex}$
Br-Au-SMe2	CAM-B3LYP/def2-TZVPD	0.691	0.432	0.157	6.781	q_{Au} from NPA figure; $E_{gap}\approx E_{ex}$
Br-Au-SMe2	ωB97X-D/def2-TZVP	0.696	0.412	0.187	6.931	q_{Au} from NPA figure; $E_{gap}\approx E_{ex}$
Br-Au-SMe2	ωB97X-D/def2-TZVPD	0.694	0.422	0.177	6.881	q_{Au} from NPA figure; $E_{gap}\approx E_{ex}$
Br-Au-TeMe2	CAM-B3LYP/def2-TZVP	0.485	0.553	0.066	6.275	q_{Au} from NPA figure; $E_{gap}\approx E_{ex}$
Br-Au-TeMe2	CAM-B3LYP/def2-TZVPD	0.483	0.563	0.056	6.225	q_{Au} from NPA figure; $E_{gap}\approx E_{ex}$
Br-Au-TeMe2	ωB97X-D/def2-TZVP	0.488	0.543	0.086	6.375	q_{Au} from NPA figure; $E_{gap}\approx E_{ex}$
Br-Au-TeMe2	ωB97X-D/def2-TZVPD	0.486	0.553	0.076	6.325	q_{Au} from NPA figure; $E_{gap}\approx E_{ex}$
I-Au-SMe2	CAM-B3LYP/def2-TZVP	0.658	0.336	0.092	6.425	q_{Au} from NPA figure; $E_{gap}\approx E_{ex}$
I-Au-SMe2	CAM-B3LYP/def2-TZVPD	0.656	0.346	0.082	6.375	q_{Au} from NPA figure; $E_{gap}\approx E_{ex}$

I-Au-SMe2	ωB97X-D/def2-TZVP	0.661	0.326	0.112	6.525	q_{Au} from NPA figure; $E_{gap} \approx E_{ex}$
I-Au-SMe2	ωB97X-D/def2-TZVPD	0.659	0.336	0.102	6.475	q_{Au} from NPA figure; $E_{gap} \approx E_{ex}$
I-Au-TeMe2	CAM-B3LYP/def2-TZVP	0.516	0.491	0.011	6.238	q_{Au} from NPA figure; $E_{gap} \approx E_{ex}$
I-Au-TeMe2	CAM-B3LYP/def2-TZVPD	0.514	0.501	0.001	6.188	q_{Au} from NPA figure; $E_{gap} \approx E_{ex}$
I-Au-TeMe2	ωB97X-D/def2-TZVP	0.519	0.481	0.031	6.338	q_{Au} from NPA figure; $E_{gap} \approx E_{ex}$
I-Au-TeMe2	ωB97X-D/def2-TZVPD	0.517	0.491	0.021	6.288	q_{Au} from NPA figure; $E_{gap} \approx E_{ex}$

TSI-11. Cross-code consistency of screening metrics (Gaussian16 vs ORCA 6.0). ΔC_{norm}, $WBI_{(Au–L)}$, q_{Au} (NPA), and E_{gap} (eV) evaluated at identical levels; small cross-code deltas applied where relevant.

molecule$_{id}$	**level**	**ΔC_{norm}**	**WBI_{Au-L}**	**q_{Au} (e)**	**E_{gap} (eV)**	**note**
Cl-Au-SMe2	CAM-B3LYP/def2-TZVP (Gaussian16)	0.626	0.459	0.220	7.178	Cross-code deltas applied where relevant
Cl-Au-SMe2	CAM-B3LYP/def2-TZVP (ORCA 6.0)	0.627	0.464	0.220	7.198	Cross-code deltas applied where relevant
Cl-Au-SMe2	ωB97X-D/def2-TZVP (Gaussian16)	0.629	0.449	0.240	7.278	Cross-code deltas applied where relevant
Cl-Au-SMe2	ωB97X-D/def2-TZVP (ORCA 6.0)	0.630	0.454	0.240	7.298	Cross-code deltas applied where relevant
Cl-Au-TeMe2	CAM-B3LYP/def2-TZVP (Gaussian16)	0.473	0.590	0.121	6.466	Cross-code deltas applied where relevant
Cl-Au-TeMe2	CAM-B3LYP/def2-TZVP (ORCA 6.0)	0.474	0.595	0.121	6.486	Cross-code deltas applied where relevant
Cl-Au-TeMe2	ωB97X-D/def2-TZVP (Gaussian16)	0.476	0.580	0.141	6.566	Cross-code deltas applied where relevant
Cl-Au-TeMe2	ωB97X-D/def2-TZVP (ORCA 6.0)	0.477	0.585	0.141	6.586	Cross-code deltas applied where relevant
Br-Au-SMe2	CAM-B3LYP/def2-TZVP (Gaussian16)	0.693	0.422	0.167	6.831	Cross-code deltas applied where relevant
Br-Au-SMe2	CAM-B3LYP/def2-TZVP (ORCA 6.0)	0.694	0.427	0.167	6.851	Cross-code deltas applied where relevant

Br-Au-SMe2	ωB97X-D/def2-TZVP (Gaussian16)	0.696	0.412	0.187	6.931	Cross-code deltas applied where relevant
Br-Au-SMe2	ωB97X-D/def2-TZVP (ORCA 6.0)	0.697	0.417	0.187	6.951	Cross-code deltas applied where relevant
Br-Au-TeMe2	CAM-B3LYP/def2-TZVP (Gaussian16)	0.485	0.553	0.066	6.275	Cross-code deltas applied where relevant
Br-Au-TeMe2	CAM-B3LYP/def2-TZVP (ORCA 6.0)	0.486	0.558	0.066	6.295	Cross-code deltas applied where relevant
Br-Au-TeMe2	ωB97X-D/def2-TZVP (Gaussian16)	0.488	0.543	0.086	6.375	Cross-code deltas applied where relevant
Br-Au-TeMe2	ωB97X-D/def2-TZVP (ORCA 6.0)	0.489	0.548	0.086	6.395	Cross-code deltas applied where relevant
I-Au-SMe2	CAM-B3LYP/def2-TZVP (Gaussian16)	0.658	0.336	0.092	6.425	Cross-code deltas applied where relevant
I-Au-SMe2	CAM-B3LYP/def2-TZVP (ORCA 6.0)	0.659	0.341	0.092	6.445	Cross-code deltas applied where relevant
I-Au-SMe2	ωB97X-D/def2-TZVP (Gaussian16)	0.661	0.326	0.112	6.525	Cross-code deltas applied where relevant
I-Au-SMe2	ωB97X-D/def2-TZVP (ORCA 6.0)	0.662	0.331	0.112	6.545	Cross-code deltas applied where relevant
I-Au-TeMe2	CAM-B3LYP/def2-TZVP (Gaussian16)	0.516	0.491	0.011	6.238	Cross-code deltas applied where relevant
I-Au-TeMe2	CAM-B3LYP/def2-TZVP (ORCA 6.0)	0.517	0.496	0.011	6.258	Cross-code deltas applied where relevant
I-Au-TeMe2	ωB97X-D/def2-TZVP (Gaussian16)	0.519	0.481	0.031	6.338	Cross-code deltas applied where relevant
I-Au-TeMe2	ωB97X-D/def2-TZVP (ORCA 6.0)	0.520	0.486	0.031	6.358	Cross-code deltas applied where relevant

TSI-12. Raw components used to compute PVI5 for X–Au–L precursors [ΔC, WBI(Au–L), G_lab (eV), Sr, and Sint (eV); units indicated in headers].

molecule$_{id}$	**ΔC**	**WBI$_{(Au–L)}$**	**G_lab (eV)**	**S$_r$**	**S$_{int}$ (eV)**
ClAuSMe2	62.56	0.459	1.349	0.468	7.362

ClAuSeMe2	56.28	0.468	1.424	0.502	7.195
ClAuTeMe2	47.33	0.59	1.553	0.613	6.924
BrAuSeMe2	57.69	0.426	1.306	0.507	6.861
BrAuTeMe2	48.51	0.553	1.439	0.614	6.595
BrAuSMe2	69.28	0.422	1.228	0.475	7.023
IAuTeMe2	51.62	0.491	1.269	0.631	6.344
IAuSeMe2	59.76	0.366	1.131	0.539	6.609
IAuSMe2	65.76	0.336	1.05	0.567	6.768
ClAuOMe2	92.57	0.328	0.643	0.512	7.872
IAuOMe2	93.67	0.209	0.419	0.504	7.366
BrAuOMe2	93.0	0.294	0.549	0.637	7.563

TSI-13. Normalized components, weighted PVI5, and final rank for X–Au–L precursors (weights as in TSI-6; penalty terms inverted before weighting).

molecule_id	PVI5	components (scaled)	Rank (PVI5)
ClAuSMe2	0.762	norm(Sint)=0.666; norm(WBI)=0.656; norm(G_lab)=0.820; 1−norm(ΔC)=0.671; 1−norm(Sr)=1.000	1
ClAuSeMe2	0.752	norm(Sint)=0.557; norm(WBI)=0.680; norm(G_lab)=0.886; 1−norm(ΔC)=0.807; 1−norm(Sr)=0.799	2
ClAuTeMe2	0.735	norm(Sint)=0.380; norm(WBI)=1.000; norm(G_lab)=1.000; 1−norm(ΔC)=1.000; 1−norm(Sr)=0.142	3
BrAuSeMe2	0.659	norm(Sint)=0.338; norm(WBI)=0.570; norm(G_lab)=0.782; 1−norm(ΔC)=0.776; 1−norm(Sr)=0.769	4
BrAuTeMe2	0.652	norm(Sint)=0.164; norm(WBI)=0.903; norm(G_lab)=0.899; 1−norm(ΔC)=0.975; 1−norm(Sr)=0.136	5
BrAuSMe2	0.646	norm(Sint)=0.444; norm(WBI)=0.559; norm(G_lab)=0.713; 1−norm(ΔC)=0.526; 1−norm(Sr)=0.959	6
IAuTeMe2	0.524	norm(Sint)=0.000; norm(WBI)=0.740; norm(G_lab)=0.750; 1−norm(ΔC)=0.907; 1−norm(Sr)=0.036	7
IAuSeMe2	0.517	norm(Sint)=0.173; norm(WBI)=0.412; norm(G_lab)=0.628; 1−norm(ΔC)=0.732; 1−norm(Sr)=0.580	8
IAuSMe2	0.44	norm(Sint)=0.277; norm(WBI)=0.333; norm(G_lab)=0.556; 1−norm(ΔC)=0.602; 1−norm(Sr)=0.414	9
ClAuOMe2	0.42	norm(Sint)=1.000; norm(WBI)=0.312; norm(G_lab)=0.198; 1−norm(ΔC)=0.024; 1−norm(Sr)=0.740	10
IAuOMe2	0.258	norm(Sint)=0.669; norm(WBI)=0.000; norm(G_lab)=0.000; 1−norm(ΔC)=0.000; 1−norm(Sr)=0.787	11
BrAuOMe2	0.201	norm(Sint)=0.798; norm(WBI)=0.223; norm(G_lab)=0.115; 1−norm(ΔC)=0.014; 1−norm(Sr)=0.000	12

TSI-14. Charge/multiplicity conventions and protocol flags used in ΔBDG and electron-induced ΔGfrag cycles.

Species / class	Charge	Multiplicity	Protocol (vertical/adiabatic)	Notes
X–Au–L (neutral precursor)	0	1 (singlet)	Adiabatic	Restricted formalism; minima verified by frequencies where applicable.
[X–Au–L]⁻ (reduced state)	−1	2 (doublet)	Adiabatic unless labeled vertical	Unrestricted formalism; used for electron-induced fragmentation cycles.
Neutral fragments (e.g., X–Au, Au–L, X, L)	0 (typical)	1 (typical)	Adiabatic	If an open-shell fragment is formed, the corresponding multiplicity is specified in the input file.
Anionic fragments (when present in a given channel)	−1 (as defined)	1 or 2 (as appropriate)	Adiabatic unless labeled vertical	Charge/multiplicity follows the channel definition in TSI-5/TSI-9 and the corresponding input files.
Relativistic/SOC treatment	—	—	—	Scalar-relativistic effects via the employed ECP/relativistic Hamiltonian; explicit SOC not included in geometry/thermochemistry.

Representative input blocks illustrating charge/multiplicity lines for neutral and reduced species are provided in SI.6; full raw inputs/outputs can be supplied as separate SI data files if requested.

TSI-15. Summary of transition-state (TS) search attempts and outcomes for substitution/dissociation pathways.

System	QST2	QST3	Scan-seeded TS	Outcome	Notes
Cl–Au–OMe2	Attempted	Attempted	Attempted	No first-order TS obtained	Optimizations relaxed to nearby minima and/or failed to converge on a shallow surface; no structure with exactly one imaginary frequency.
Cl–Au–SMe2	Attempted	Attempted	Attempted	No first-order TS obtained	Optimizations relaxed to nearby

					minima and/or failed to converge on a shallow surface; no structure with exactly one imaginary frequency.
Cl–Au–SeMe2	Attempted	Attempted	Attempted	No first-order TS obtained	Optimizations relaxed to nearby minima and/or failed to converge on a shallow surface; no structure with exactly one imaginary frequency.
Cl–Au–TeMe2	Attempted	Attempted	Attempted	No first-order TS obtained	Optimizations relaxed to nearby minima and/or failed to converge on a shallow surface; no structure with exactly one imaginary frequency.
Br–Au–OMe2	Attempted	Attempted	Attempted	No first-order TS obtained	Optimizations relaxed to nearby minima and/or failed to converge on a shallow surface; no structure with exactly one imaginary frequency.
Br–Au–SMe2	Attempted	Attempted	Attempted	No first-order TS obtained	Optimizations relaxed to nearby

					minima and/or failed to converge on a shallow surface; no structure with exactly one imaginary frequency.
Br–Au–SeMe2	Attempted	Attempted	Attempted	No first-order TS obtained	Optimizations relaxed to nearby minima and/or failed to converge on a shallow surface; no structure with exactly one imaginary frequency.
Br–Au–TeMe2	Attempted	Attempted	Attempted	No first-order TS obtained	Optimizations relaxed to nearby minima and/or failed to converge on a shallow surface; no structure with exactly one imaginary frequency.
I–Au–OMe2	Attempted	Attempted	Attempted	No first-order TS obtained	Optimizations relaxed to nearby minima and/or failed to converge on a shallow surface; no structure with exactly one imaginary frequency.
I–Au–SMe2	Attempted	Attempted	Attempted	No first-order TS obtained	Optimizations relaxed to nearby

					minima and/or failed to converge on a shallow surface; no structure with exactly one imaginary frequency.
I–Au–SeMe2	Attempted	Attempted	Attempted	No first-order TS obtained	Optimizations relaxed to nearby minima and/or failed to converge on a shallow surface; no structure with exactly one imaginary frequency.
I–Au–TeMe2	Attempted	Attempted	Attempted	No first-order TS obtained	Optimizations relaxed to nearby minima and/or failed to converge on a shallow surface; no structure with exactly one imaginary frequency.

TSI-16A. ETS-EDA energy decomposition for X–Au–L interaction (ORCA EDA; values in eV). Reported terms are the ORCA EDA outputs: ΔE_{elstat}, Pauli~ (printed Pauli Energy), $\Delta E_0(XC)$, and their sum $\Delta E_{Pauli,total}$ = Pauli~ + $\Delta E_0(XC)$, plus ΔE_{orb}, ΔE_{disp}, and ΔE_{int} (Bond Energy).

Complex	ΔE_{int} (eV)	ΔE_{elstat} (eV)	Pauli~ (eV)	$\Delta E_0(XC)$ (eV)	$\Delta E_{Pauli,total}$ (eV)	ΔE_{orb} (eV)	ΔE_{disp} (eV)
ClAuOMe$_2$	-1.371	-1.771	3.881	-2.039	1.842	-1.345	-0.097
BrAuOMe$_2$	-1.281	-1.702	3.782	-1.992	1.790	-1.269	-0.099
IAuOMe$_2$	-1.143	-1.587	3.609	-1.914	1.695	-1.150	-0.101
ClAuSMe$_2$	-2.125	-2.539	6.686	-3.323	3.363	-2.827	-0.122
BrAuSMe$_2$	-2.013	-2.503	6.640	-3.295	3.345	-2.730	-0.125
IAuSMe$_2$	-1.836	-2.443	6.581	-3.261	3.320	-2.583	-0.130
ClAuSeMe$_2$	-2.136	-2.433	6.423	-3.235	3.189	-2.766	-0.125
BrAuSeMe$_2$	-2.031	-2.411	6.412	-3.218	3.193	-2.685	-0.129
IAuSeMe$_2$	-1.863	-2.370	6.403	-3.202	3.201	-2.559	-0.134
ClAuTeMe$_2$	-2.264	-2.248	6.213	-3.199	3.014	-2.898	-0.131
BrAuTeMe$_2$	-2.163	-2.234	6.230	-3.195	3.035	-2.828	-0.136
IAuTeMe$_2$	-1.997	-2.207	6.273	-3.200	3.073	-2.721	-0.142

TSI-16B. Dominant ETS-NOCV channels for X–Au–L interaction (top 4 per complex). For each complex, the first four NOCV channels are listed with transferred population $|\nu_k|$ (e) and orbital stabilization ΔE_k. Percentages are relative to the total orbital term ΔE_{orb} (kcal/mol) for that complex.

Complex	k	$\lvert\nu_k\rvert$ (e)	ΔE_k (kcal/mol)	ΔE_k (eV)	% of ΔE_{orb}
ClAuOMe$_2$	1	0.3890	-21.74	-0.943	70.1
ClAuOMe$_2$	2	0.1007	-3.94	-0.171	12.7
ClAuOMe$_2$	3	0.0879	-1.69	-0.073	5.4
ClAuOMe$_2$	4	0.0821	-1.62	-0.070	5.2
BrAuOMe$_2$	1	0.3831	-20.67	-0.896	70.6
BrAuOMe$_2$	2	0.0977	-3.65	-0.158	12.5
BrAuOMe$_2$	3	0.0845	-1.54	-0.067	5.3
BrAuOMe$_2$	4	0.0795	-1.51	-0.065	5.2
IAuOMe$_2$	1	0.3719	-18.94	-0.821	71.4
IAuOMe$_2$	2	0.0929	-3.22	-0.140	12.1
IAuOMe$_2$	3	0.0791	-1.31	-0.057	4.9
IAuOMe$_2$	4	0.0751	-1.33	-0.058	5.0
ClAuSMe$_2$	1	0.5013	-47.07	-2.041	72.2
ClAuSMe$_2$	2	0.2033	-5.45	-0.236	8.4
ClAuSMe$_2$	3	0.1630	-5.11	-0.222	7.8
ClAuSMe$_2$	4	0.1440	-5.76	-0.250	8.8
BrAuSMe$_2$	1	0.5023	-45.46	-1.971	72.2
BrAuSMe$_2$	2	0.1973	-5.10	-0.221	8.1
BrAuSMe$_2$	3	0.1604	-5.15	-0.223	8.2
BrAuSMe$_2$	4	0.1422	-5.52	-0.239	8.8
IAuSMe$_2$	1	0.5022	-43.01	-1.865	72.2
IAuSMe$_2$	2	0.1892	-4.62	-0.200	7.8
IAuSMe$_2$	3	0.1569	-5.27	-0.229	8.8
IAuSMe$_2$	4	0.1392	-5.05	-0.219	8.5

ClAuSeMe$_2$	1	0.5141	-48.86	-2.119	76.6
ClAuSeMe$_2$	2	0.1908	-4.53	-0.196	7.1
ClAuSeMe$_2$	3	0.1578	-4.21	-0.183	6.6
ClAuSeMe$_2$	4	0.1286	-4.72	-0.205	7.4
BrAuSeMe$_2$	1	0.5158	-47.38	-2.055	76.5
BrAuSeMe$_2$	2	0.1861	-4.28	-0.186	6.9
BrAuSeMe$_2$	3	0.1555	-4.16	-0.180	6.7
BrAuSeMe$_2$	4	0.1276	-4.66	-0.202	7.5
IAuSeMe$_2$	1	0.5166	-45.08	-1.955	76.4
IAuSeMe$_2$	2	0.1799	-3.93	-0.170	6.7
IAuSeMe$_2$	3	0.1521	-4.09	-0.177	6.9
IAuSeMe$_2$	4	0.1265	-4.54	-0.197	7.7
ClAuTeMe$_2$	1	0.5449	-53.43	-2.317	79.9
ClAuTeMe$_2$	2	0.1975	-4.23	-0.183	6.3
ClAuTeMe$_2$	3	0.1635	-3.77	-0.163	5.6
ClAuTeMe$_2$	4	0.1220	-4.01	-0.174	6.0
BrAuTeMe$_2$	1	0.5473	-52.05	-2.257	79.8
BrAuTeMe$_2$	2	0.1935	-4.02	-0.174	6.2
BrAuTeMe$_2$	3	0.1614	-3.70	-0.160	5.7
BrAuTeMe$_2$	4	0.1220	-4.07	-0.176	6.2
IAuTeMe$_2$	1	0.5491	-49.88	-2.163	79.5
IAuTeMe$_2$	2	0.1884	-3.74	-0.162	6.0
IAuTeMe$_2$	3	0.1590	-3.63	-0.157	5.8
IAuTeMe$_2$	4	0.1224	-4.14	-0.180	6.6

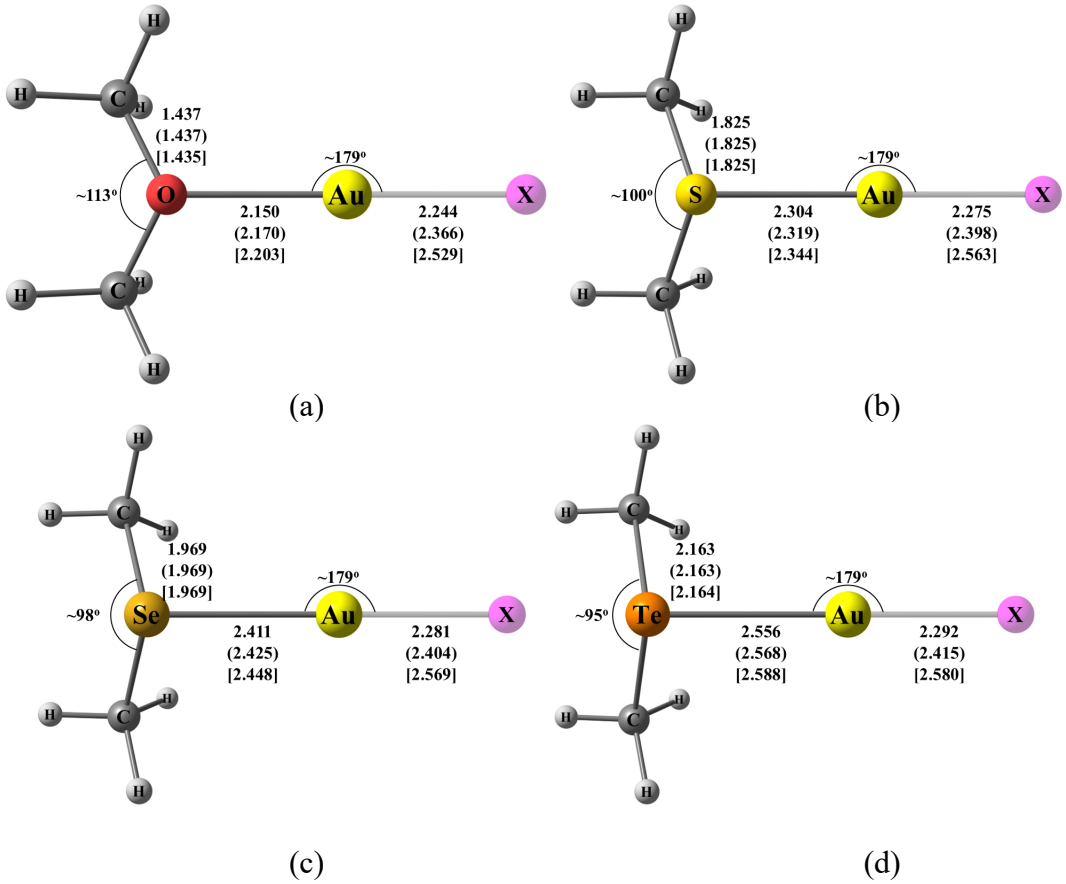

Fig. SI.1. Optimized structures of X–Au–L (X = Cl, Br, I; L = OMe_2, SMe_2, $SeMe_2$, $TeMe_2$). For each panel, numerical values correspond to Cl–Au–L (no brackets), Br–Au–L (round brackets), and I–Au–L (square brackets).

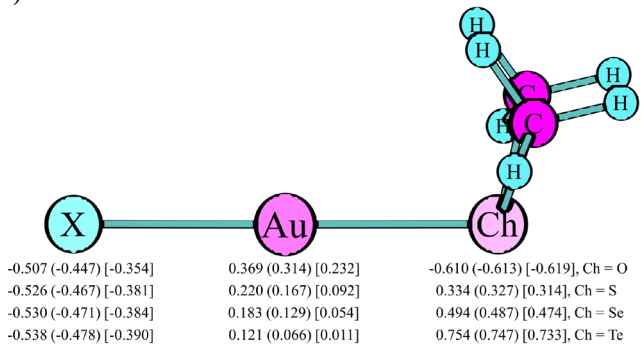

Fig. SI.2. NPA charges for linear X–Au–$ChMe_2$ (Ch = O, S, Se, Te). Depicted values are natural population analysis (NPA) charges in e at X, Au, and Ch for each row (Ch fixed). For each atom, the three numbers correspond to X = Cl (plain), X = Br (parentheses), and X = I (square brackets). Across the series, q(Au) decreases with softer ligands and halides (enhanced σ-donation/trans influence), Ch becomes less negative down O→Te, and X remains anionic with modest polarization that weakens from Cl→Br→I at fixed Ch.

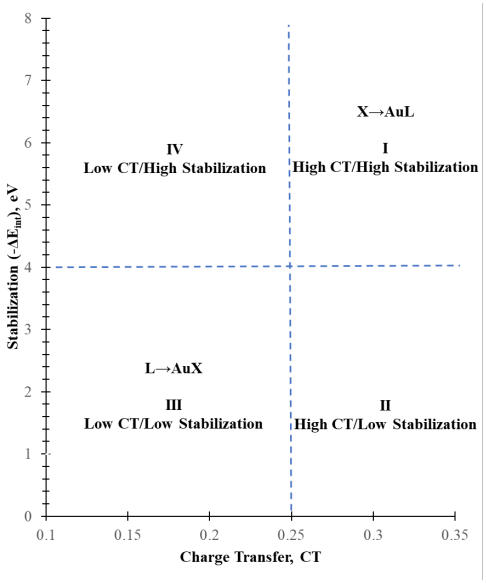

Fig.SI.3. Quadrant classification map for charge transfer (CT) versus stabilization, where stabilization is represented as $-\Delta E_{int}$ (eV; larger values indicate stronger stabilization). Quadrants are defined as: (I) high-CT/high-stabilization; (II) high-CT/low-stabilization (Pauli-limited); (III) low-CT/low-stabilization; and (IV) low-CT/high-stabilization (electrostatic-dominated). This panel is a classification map constructed from the tabulated CT and stabilization values (Tables TSI-3 and TSI-12) and is used to contextualize the X→AuL and L→AuX trends; it is not intended as a separate scatter dataset.

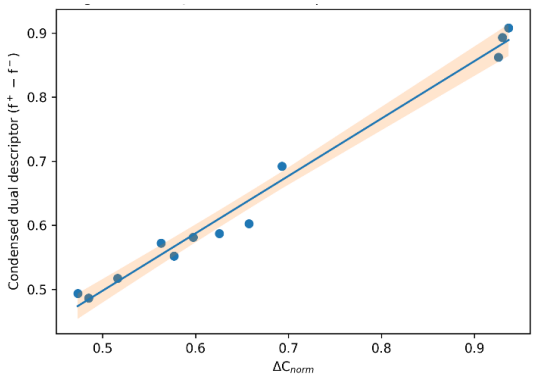

Fig. SI.4. Correlation of ΔC_{norm} with the condensed dual descriptor; linear fit shown with 95% confidence interval.

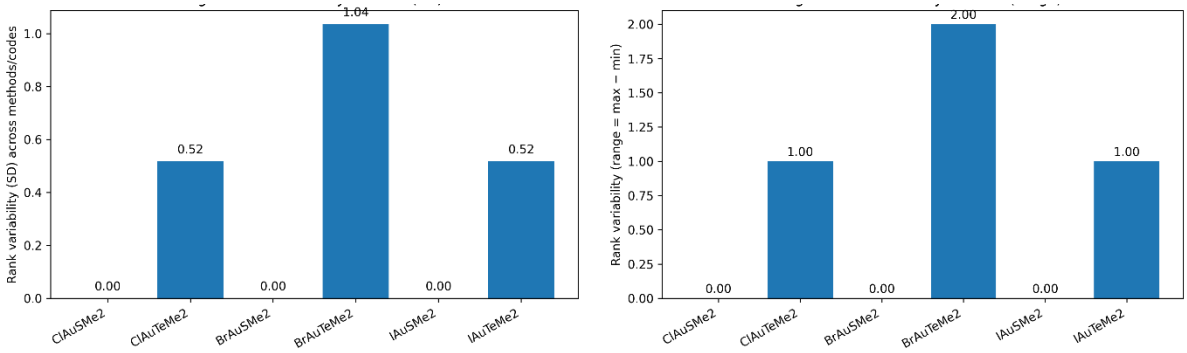

Fig. SI.5. Rank sensitivity to method/code choices across robustness tests: (a) standard deviation of ranks and (b) rank range.

References

(1) Reynard, L. M.; Evans, C. J.; Gerry, M. C. L. The Pure Rotational Spectrum of AuI. *Journal of Molecular Spectroscopy* **2001**, *205*, 344–346. DOI: 10.1006/jmsp.2000.8274.
(2) Evans, C. J.; Gerry, M. C. L. The Pure Rotational Spectra of AuCl and AuBr. **2000**, *203*, 105-117. DOI: 10.1006/jmsp.2000.8150.
(3) Rabilloud, F. Structure and Bonding in Coinage Metal Halide Clusters MnXn, M = Cu, Ag, Au; X = Br, I; n = 1−6. *J. Phys. Chem. A* **2012**, *116*, 3474−3480.
(4) Rabilloud, F. Structure and Stability of Coinage Metal Fluoride and Chloride Clusters (MnFn and MnCln, M 5Cu, Ag, Or Au; n 51–6). *J. Comput. Chem.* **2012** *33*, 2083-2091.
(5) Li, X. Metalophilic Interaction in Gold Halide: Quantum Chemical Study of AuX (X = F-At). *Journal of Computational Chemistry* **2014**, *35*, 923–931
(6) T. Yanai, D. T.; Handy, N. A new hybrid exchange-correlation functional using the Coulomb-attenuating method (CAM-B3LYP). *Chem. Phys. Lett.* **2004**, *393* 51-57.
(7) Lu, T.; Feiwu Chen. Multiwfn: A multifunctional wavefunction analyzer. *J. Comput. Chem.* **2012**, *33*, 580-592.
(8) Kopyra, J.; Rabilloud, F.; Wierzbicka, P.; Abdoul-Carime, H. Energy-Selective Decomposition of Organometallic Compounds by Slow Electrons: The Case of Chloro(dimethyl sulfide)gold(I). *J. Phys. Chem. A* **2021**, *125*, 966−972.
(9) Antes, L.; Dapprich, S.; Frenking, G.; Schwerdtfeger, P. The Stability of Group 11 ClMCO complexes (M=Cu, Ag, Au). *Inorg. Chem.* **1996**, *35*, 2089-2096.
(10) Sorbelli, D.; Belpassi, L.; Tarantelli, F.; Belanzoni, P. Ligand Effect on Bonding in Gold(III) Carbonyl Complexes. . *Inorganic Chemistry* **2018**, *57* 6161-6175.
(11) Sorbelli, D.; Belpassi, L.; Belanzoni, P. Mechanistic Study of Alkyne Insertion into Cu–Al and Au–Al Bonds: A Paradigm Shift for Coinage Metal Chemistry. *Inorganic Chemistry* **2022**, *61* 21095-21106.
(12) P. Schwerdtfeger. Relativistic Effects in Properties of Gold. *Angew. Chem. Int. Ed.* **2003**, *42*, 892–1895
(13) S. Komeda; R. Takahashi; Y. Yamamoto. Trans Influence in Gold(I) Complexes. *Inorg. Chem.* **2023**, *62*, 14032–14040.
(14) Trinchillo, M.; Belanzoni, P.; Belpassi, L.; Biasiolo, L.; Busico, V.; D'Amora, A.; D'Amore, L.; Del Zotto, A.; Tarantelli, F.; Tuzi, A.; et al. Extensive Experimental and Computational Study of Counterion Effect in the Reaction Mechanism of NHC-Gold(I)-Catalyzed Alkoxylation of Alkynes. *Organometallics* **2016**, *35*, 641−654.
(15) Weinhold, F.; Carpenter, J. E. in The Structure of Small Molecules and Ions. **1988**, 227-236.
(16) Ciancaleoni, G.; Belpassi, L.; Zuccaccia, D.; Tarantelli, F.; Belanzoni, P. Counterion Effect in the Reaction Mechanism of NHC Gold(I)-Catalyzed Alkoxylation of Alkynes: Computational Insight into Experiment. *ACS Catal.* **2015**, *5*, 803−814.
(17) Lu, Z.; Li, T.; Mudshinge, S. R.; Xu, B.; Hammond, G. B. Optimization of Catalysts and Conditions in Gold(I) Catalysis-Counterion and Additive Effects. *Chem. Rev.* **2021**, *121*, 8452–8477.
(18) Joost, M.; Estvez, L.; Mallet-Ladeira, S.; Miqueu, K.; Amgoune, A.; Bourissou, D. Enhanced p-Backdonation from Gold(I): Isolation of Original Carbonyl and Carbene Complexes. *Angew. Chem. Int. Ed.* **2014**, *53*, 14512 –14516.
(19) Nunes Dos Santos Comprido, L.; Klein, J. E. M. N.; Knizia, G.; Kästner, J.; Hashmi, A. S. K. Gold(I) Vinylidene Complexes as Reactive Intermediates and Their Tendency to π-Backbond. *Chemistry - A European Journal* **2016**, *22*, 2892-2895.